The Impact of Core/Shell Sizes on the Optical Gain Characteristics of CdSe/CdS Quantum Dots

Suzanne Bisschop, Pieter Geiregat, Tangi Aubert, Zeger Hens

The Impact of Core/Shell Sizes on the Optical Gain Characteristics of CdSe/CdS Quantum Dots

Suzanne Bisschop,[†,‡] Pieter Geiregat,[†,‡] Tangi Aubert,[†,‡] and Zeger Hens[*,†,‡]

Physics and Chemistry of Nanostructures, Ghent University, Belgium, and Center for Nano and Biophotonics (NB Photonics), Ghent University, Belgium

E-mail: zeger.hens@ugent.be

Abstract

Colloidal quantum dots (QDs) are highly attractive as the active material for optical amplifiers and lasers. Here, we address the relation between the structure of CdSe/CdS core/shell QDs, the material gain they can deliver and the threshold needed to attain net stimulated emission by optical pumping. Based on an initial gain model, we predict that reducing the thickness of the CdS shell grown around a given CdSe core will increase the maximal material gain, while increasing the shell thickness will lower the gain threshold. We assess this trade-off by means of transient absorption spectroscopy. Our results confirm that thin-shell QDs exhibit the highest material gain. In quantitative agreement with the model, core and shell sizes hugely impact on the material gain, which ranges from 2800 cm^{-1} for large core/thin shell QDs to less than 250 cm^{-1} for small core/thick shell QDs. On the other hand, the significant threshold reduction expected for thick-shell QDs is absent. We relate this discrepancy between model

*To whom correspondence should be addressed
†Physics and Chemistry of Nanostructures, Ghent University, Belgium
‡Center for Nano and Biophotonics (NB Photonics), Ghent University, Belgium

and experiment to a transition from attractive to repulsive exciton-exciton interactions with increasing shell thickness. The spectral blueshift that comes with exciton-exciton repulsion leads to competition between stimulated emission and higher energy absorbing transition, which raises the gain threshold. As a result, small-core/thick-shell QDs need up to 3.7 excitations per QD to reach transparency, whereas large-core/thin shell QDs only need 1.0, a number often seen as a hard limit for biexciton-mediated optical gain. This makes large-core/thin-shell QDs that feature attractive exciton-exciton interactions the overall champion core/shell configuration in view of highest material gain, lowest threshold exciton occupation and longest gain lifetime.

Keywords

nanocrystals, heterostructures, ultrafast spectroscopy, stimulated emission, material gain, lasers

Optical gain in quasi-spherical colloidal semiconductor nanocrystals or quantum dots (QDs) was demonstrated shortly after the development of synthesis methods that yielded monodisperse QD dispersions.[1] Since QDs combine size-tunable optical properties with a suitability for solution-based processing, they are highly attractive nanomaterials for optical amplifiers and lasers.[2] Soon after the first successful demonstration of optical gain in colloidal QDs, their integration within dielectric host materials to make optically pumped solid-state QD-lasers became a subject of intense research and several research groups were able to demonstrate lasing action under pulsed optical excitation using different cavity designs.[3–7] Follow-up efforts have resulted in considerable improvements in the overall lasing performance by reducing the lasing threshold,[8–11] but it was not until recently that also (quasi) continuous-wave optical amplification and lasing devices were demonstrated.[12–15]

The step towards actual device development leads almost naturally to the question of optimization, *i.e.*, the development of QD-lasers featuring, for example, a minimized lasing threshold or device footprint. Meaningful optimization, however, requires (1) a framework that translates optical gain by quantum dots into a measurable and reproducible quantity, (2) a microscopic model that links optical gain to the opto-electronic properties – and thus the structure – of individual QDs, and (3) device-level simulations to model and quantify lasing action. In literature, especially the second point has been deeply studied from the perspective of the population inversion lifetime. Early work on CdSe-based QDs showed that net optical gain results from so-called biexcitons, which recombine rapidly through non-radiative Auger processes.[16] Especially in the case of CdSe/CdS core/shell QDs, it proved possible to limit Auger recombination rates by developing thick shell QDs with an alloyed core/shell interface.[17–21] These results made possible the development of QD-based lasers that work under nanosecond and continuous-wave optical pumping.[13,14] The role of Auger recombination was further addressed recently at the level of device simulations by Park *et al.*[22] These authors use a simplified model QD featuring 2-fold degenerate band-edge states to link a reduction of the Auger recombination rate to a lowering of lasing thresholds under pulsed and continuous-wave optical pumping.

The initial reports on optical gain by QDs expressed the condition to reach stimulated emission in terms of the gain cross section and the population inversion decay rate, which was dictated by Auger recombination.[1] As discussed above, the optimization of QDs for lasing applications has mainly focused on strategies to slow down Auger recombination. On the other hand, the development of microlasers based on CdSe/CdS core/shell QDs highlighted the role of the material gain to reach lasing action.[23–27] Taking the case of integrated microdisks lasers proposed by Xie *et al.*,[24] lasing was only attained in sufficiently large resonators, in which the modal gain countered the optical losses. This makes that the material gain is a quantity that must be addressed, next to the lasing threshold and the population inversion lifetime, when optimizing QDs for optical gain. Thinking of core/shell

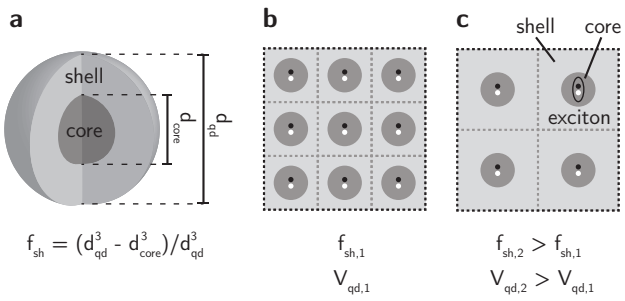

Figure 1: (a) Schematic representation of a core/shell QD (b) Cartoon of a film consisting of densely packed (volume fraction $f = 1$) core/shell QDs. For simplicity, shells have been given a square geometry and electron-hole pairs are depicted by a combination of a black and a white dot. (c) Same volume filled with core/shell QDs that have an identical core as in (b) but a thicker shell ($f_{\mathrm{sh},2} > f_{\mathrm{sh},1}$) and thus a larger total volume ($V_{\mathrm{qd},2} > V_{\mathrm{qd},1}$). The dilution that comes with an increase of the shell volume can be readily appreciated.

QDs, this leads directly to the question as to how the material gain is related to the QD structure, *i.e.*, core size and shell thickness. For example, in the case of films of core/shell QDs as shown in Figure 1, an increase of the shell volume will always come at the cost of a diluted core concentration for a given core size. Since stimulated emission comes from core-related transitions, one expects a concomitant reduction of the gain coefficient of the film. At the same time, as less electron-hole pairs need to be created per unit volume, more voluminous shells could make for lower lasing thresholds, in particular when the shell can absorb pump light. Until now, however, such tradeoffs have not been experimentally verified, let alone that they have been exploited to optimize QD-lasers.

Here, we address the relation between the structure of CdSe/CdS core/shell QDs, their optical gain – which we quantify as the material gain – and the threshold needed to attain net stimulated emission. We first build on the simplified electronic structure model introduced by Park *et al.*[22] to show that increasing the shell-to-total-QD volume fraction f_{sh} should markedly reduce the gain threshold when pumping at photon energies above the band gap of the shell, at the expense of a markedly lower material gain. We analyze these predictions by means of quantitative transient absorption spectroscopy on dispersions of CdSe/CdS QDs with different core-shell geometries. It follows that thin shell QDs indeed feature the highest

gain coefficients. On the other hand, the significant threshold reduction expected for more voluminous QDs is absent. In fact, the thresholds of small-core/thick-shell QDs were found to be equal at best to those of core/shell QDs with thinner shells. Using an extended QD model to simulate the QD gain spectrum, we show that this increased gain threshold for thicker-shell QDs finds its origin in a variation of the exciton-exciton Coulomb interaction, which shifts from attractive for thin shell to repulsive for thick-shell QDs. Such shifts greatly influence the gain threshold, up to the point where large-core/thin-shell QDs, which exhibit a redshifted biexciton transition, are the overall champion core/shell configuration in terms of material gain, gain threshold and gain lifetime.

Results

Initial Estimate of the Impact of Core/Shell Sizes on Optical Gain

In this study, we analyze optical gain by means of the material gain g_i and the threshold occupation $\langle N \rangle_{\mathrm{th}}$. Similar to the intrinsic absorption coefficient,[28] the material gain is the gain coefficient of a fictitious QD composite in which the QD volume fraction is one (see Supporting Information S1).[29] The threshold occupation, on the other hand, is the average number of electron-hole pairs created per QD by a femtosecond pulse at which a QD ensemble reaches transparency. To have an initial estimate of the influence of the shell volume on these gain characteristics, we studied the relation between g_i, $\langle N \rangle_{\mathrm{th}}$ and the core/shell morphology starting from a core/shell QD model system. We characterized the core/shell morphology by the shell volume fraction f_{sh} (see Figure 1a) and we identified stimulated emission with a transition between a 2-fold degenerate upper state (conduction-band edge) and a 4-fold degenerate lower state (valence-band edge) in the QD core (see Figure 2a). While this combination of 2-fold and a 4-fold degenerate band-edge is often put forward for CdSe QDs,[30] the analysis can be readily extended to band-edge states with different degeneracies (see Supporting Information S2). To focus on the main trends, we represented the absorbance

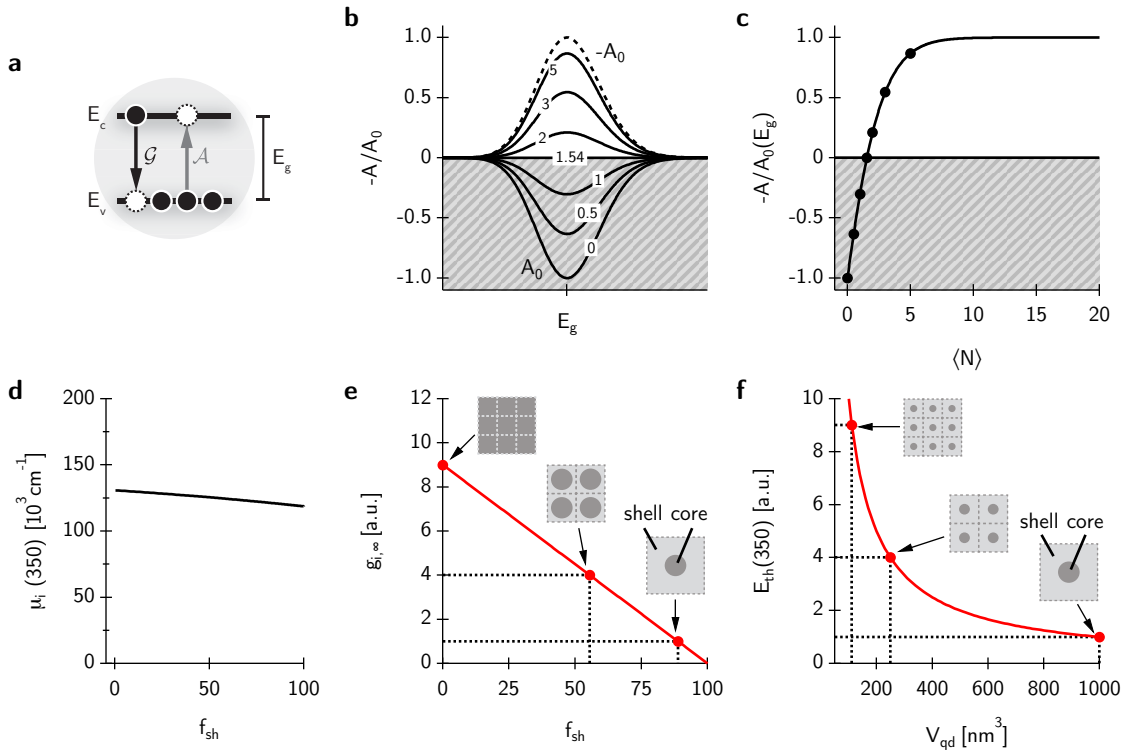

Figure 2: (a) Representation of a QD core as a 2-level system featuring valence-band and conduction-band edges with a $g_h = 4$ and $g_e = 2$ fold degeneracy, respectively. (b) $-A/A_0$ as a function of photon energy E for various electron-hole pair occupation numbers $\langle N \rangle$, indicated as trace labels. (c) Variation of $-A/A_0$ at E_g with $\langle N \rangle$, showing the gain threshold $\langle N \rangle_{\mathrm{th}} = 1.54$ and saturation at $-A/A_0 = 1$. (d) μ_i at 350 nm *vs.* f_{sh}, as calculated from bulk optical constants through Maxwell-Garnett theory. (e) Theoretically predicted $g_{i,\mathrm{max}}$ as a function of f_{sh} for core/shell QDs with a fixed core size. (f) Theoretically predicted J_{th} as a function of V_{qd} for core/shell QDs with a fixed shell volume fraction.

spectrum A_0 of the band-edge transition by a single Gaussian with central energy E_g, and simulated the corresponding non-linear absorbance A as a function of ($\langle N \rangle$). To do so, we assumed that the resulting 8 exciton states are degenerate and exhibit a rapid thermal equilibrium. Moreover, we discarded spectral shifts in photo-excited QDs and we took the oscillator strength of the band-edge transition as proportional to the number of available combinations of unoccupied valence and a conduction band-edge states.

The simulated normalized non-linear absorbance spectra are shown in Figure 2b, where $A > 0$ corresponds to net absorbance (grey area) while $A < 0$ corresponds to net stimulated emission. The evolution from net absorbance to net gain shown by Figure 2b is analyzed

further in Figure 2c, which represents $-A/A_0$ at the band-gap energy E_g as a function of $\langle N \rangle$. One sees that increasing $\langle N \rangle$ first leads to a linear reduction of the absorbance, after which a regime of net gain is reached at $\langle N \rangle = 1.54$. Finally, the normalized amplification levels off at 1 at high exciton populations, so the maximum gain attained when the system is completely inverted equals the original absorbance. Hence, the initial model indicates that the maximum material gain $g_{i,\infty}(\lambda)$ that can be attained at a given wavelength is equal to the intrinsic absorption coefficient $\mu_i(\lambda)$ of the unexcited QDs at that wavelength. In the case of CdSe/CdS QDs, $\mu_i(\lambda)$ is mostly independent of the shell volume at wavelengths shorter than the CdS band-edge transition (see Figure 2d), yet the contribution of the core to μ_i will be smaller the larger f_{sh} (see Supporting Information S2). As shown in Figure 2e, this makes that the maximum material gain linked to the CdSe core band-edge transition systematically drops when f_{sh} is raised, up to the point where it vanishes for $f_{\mathrm{sh}} \to 1$.

In view of gain thresholds, Figures 2b and c indicate that transparency is reached when $\langle N \rangle_{\mathrm{th}} = 1.54$ for the case that $g_{\mathrm{e}} = 2$ and $g_{\mathrm{h}} = 4$. Importantly, since this number only depends on the degeneracy of the band-edge states, it should be independent of the presence or not of any shell around the initial core QD. At the same time, the average number of electron-hole pairs $\langle N \rangle$ that is created per QD by a given photon flux scales with the absorption cross section σ of the QDs at the pump wavelength. Since σ is given by the product $\mu_i \times V_{\mathrm{qd}}$ of the intrinsic absorption coefficient and the QD volume, it follows that the photon flux needed to reach this threshold occupation will scale inversely with V_{qd}. This conclusion can be extended to core/shell QDs, provided that excitation wavelengths shorter than the shell band-gap transition are used, where μ_i varies only slightly with f_{sh} (see Figure 2d). As shown in Figure 2f, we thus expect a lower threshold flux for the most voluminous QDs when such pump wavelengths are used.

Table 1: Core and shell sizes of the different CdSe/CdS QD samples used for this study.

Sample	d_{c}	d_{qd}	f_{sh}
S1	4.0	7.3	84
S2	4.0	9.0	92
S3	2.9	8.6	96
S4	2.9	9.4	97
S5	2.4	10.1	99
S6	2.9	11.0	98
S7	2.3	11.8	99

CdSe/CdS Core/Shell QDs, Spectroscopic Characteristics

To assess the relations put forward between the morphology of core/shell QDs and their optical gain characteristics, we analyzed a set of 7 CdSe/CdS core/shell QDs that each have a different combination of volume V_{qd} and shell volume fraction f_{sh} (see Table 1 and Supporting Information S3 for TEM images). All samples consisted of oleate-capped core/shell QDs synthesized using a seeded-growth *flash* method as previously described in the literature.[31,32] Specific to this synthesis is that CdS shells are rapidly grown around wurtzite CdSe core QDs by heterogeneous nucleation at high temperature. The core/shell morphology is varied by changing the size of the injected core QDs, and adapting the amount of Cd and S precursor used for shell growth. The resulting QDs feature an alloyed CdSe/CdS interface,[31] which can mitigate strain and slow down non-radiative Auger recombination of multi-excitons.[18,19,31,33]

Figure 3a presents an overview of the absorbance and photoluminescence spectra of all 7 samples used in this study. Note that the sample color code introduced in Figure 3a will be used in all the following figures. In all cases, the absorbance spectra exhibit a pronounced shell-enhanced absorption at wavelengths shorter than the CdS bulk bandgap of ~ 520 nm (see Figure 3b), whereas various features that are characteristic of transitions within the core CdSe QDs can be seen at wavelengths longer than the CdS bulk bandgap. These features can be traced back more readily by means of the second derivative of the absorbance spectrum, as shown in Figure 3c for the case of sample S1. Here, the most relevant features have been assigned according to literature to transitions to the lowest conduction-band S state

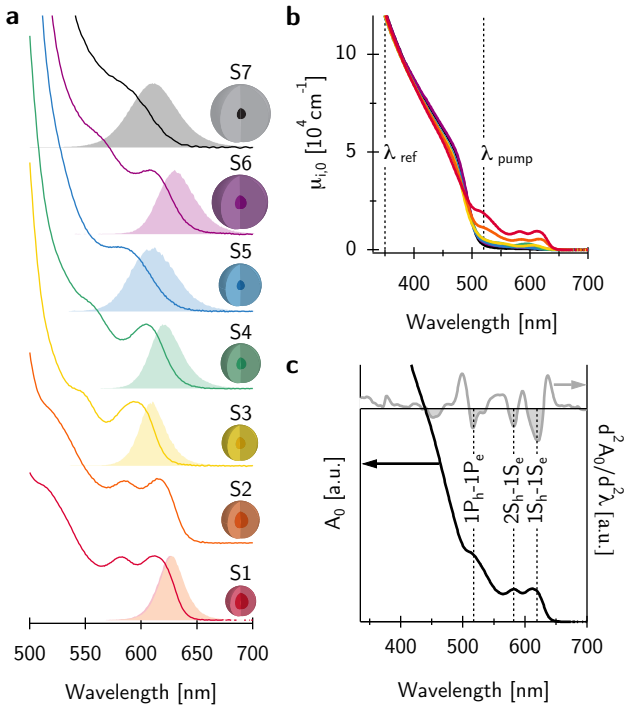

Figure 3: (a) Overview of absorbance and photoluminescence spectra for the different CdSe/CdS core/shell samples S1-S7. See Table 1 for an overview of core and shell sizes, and shell volume fraction. (b) $\mu_{i,0}$-spectra, calculated using Eq S16 and the measured absorbance (A_0) spectra. (c) Spectrum of (black) absorbance (A_0) and (grey) the second derivative of the absorbance of sample S1, with the assignment of the most relevant absorption features as indicated.

($1S_h - 1S_e$ and $2S_h - 1S_e$) or the second conduction-band P state ($1P_h - 1P_e$).[34] The emission of the different samples has a central wavelength that varies between 610 and 625 nm, and a full-width at half-maximum (FWHM) ranging between 25–48 nm, depending on core size and shell thickness. In addition, the radiative lifetime ranges between 15–54 ns, where larger nanocrystals have the longest lifetimes (see Supporting Information S4). Such characteristics are typical for colloidal CdSe/CdS QDs.

To quantify stimulated emission by CdSe/CdS QDs, we determined the non-linear absorbance $A(\lambda)$ of the different QD dispersions using pump-probe transient absorption spectroscopy (TAS). For this, stirred dispersions were excited using a 110 fs pump pulse and the change in absorbance ΔA was measured as a function of the probe wavelength and the

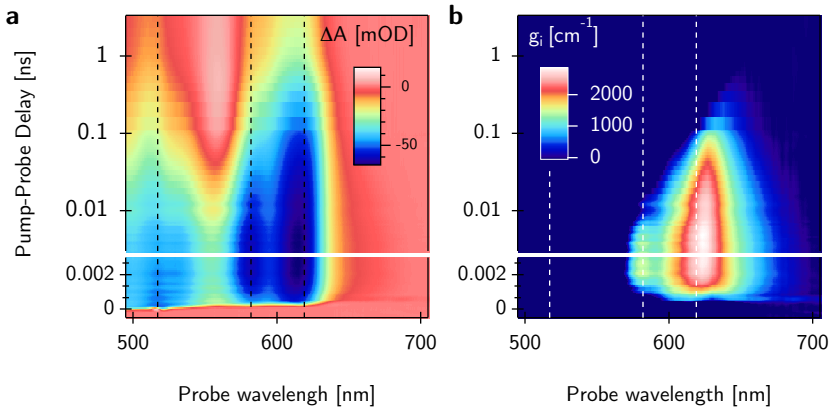

Figure 4: (a) Time-wavelength map of the differential absorbance recorded on sample S1 after optical pumping at 520 nanometer. A fluence of 0.73 mJ/cm^2 was used. (b) The concomitant map of the material gain calculated using Eq S16, showing a material gain up to 2800 cm^{-1}. In both graphs, the vertical lines indicate the spectral position of the three transitions identified in the linear absorbance spectrum (see Figure 3c).

pump-probe delay. Figure 4a shows such a 2D transient absorption map recorded on sample S1 dispersed in toluene, when pumped with 520 nm light at a pump energy fluence of 0.73 mJ/cm^2. The map is characterized by a pronounced bleach of the absorbance ($\Delta A < 0$) at wavelengths corresponding to the different core related transitions. In line with literature, we attribute this to filling of the band-edge states with photogenerated electrons and holes, such that the gradual reduction of the bleach signal is then indicative of the recombination of photo-excited multi-exciton states.[34]

By adding the linear absorbance A_0 to the transient absorbance ΔA, we obtained the non-linear absorbance A of the CdSe/CdS QDs after photoexcitation as a function of wavelength and pump-probe delay. In the resulting non-linear absorbance map, areas where $A > 0$ point to remaining absorption after photoexcitation, whereas a negative absorbance $A < 0$ is indicative of optical gain. As outlined in Supporting Information S1, such a non-linear absorbance map can be rescaled to a map of the material gain g_i, which is an intrinsic material property that enables optical gain by different samples to be compared on the same footing. Figure 4b shows the material gain map that corresponds to the ΔA map of Figure 4a. It can be seen that especially around the band-edge transition, the aforementioned bleach

feature reflects a situation of optical gain. More specifically, we find that the used conditions of optical pumping lead to a gain band that is more than 100 nm wide, centred around the first $1S_h - 1S_e$ transition, and that lasts up to 600 ps. Moreover, we find a maximum material gain in this case of 2800 cm^{-1}.

To study the time constants of the decay of the photo-excited state, we analyzed the non-linear absorbance at the band-edge as a function of pump-probe delay for different pump powers. To obtain the lifetime of the various multi-exciton states, we fitted such decay traces to a sum of exponentials, while constraining the decay rates such that they reflect the known scaling of Auger recombination rates with the exciton number (see Supporting Information S5).[35] Depending on the core and shell dimensions, this yielded a biexciton lifetime ranging from 190 to 390 ps. Moreover, considering sets of samples with similar core sizes, such as (S1; S2), (S3; S4; S6), and (S5; S7), we systematically find that the biexciton lifetime increases with increasing QD volume. Such values and trends are in line with literature reports on the biexciton lifetime in CdSe/CdS QDs,[23] and they are comparable to the time span net gain is maintained after pumping (see Figure 4b). In line with literature, we thus assign the optical gain observed after photo-excitation of CdSe/CdS QDs to stimulated emission from bi- or multi-excitons states.[22,34]

Quantitative Analysis of Optical Gain

By means of material gain maps recorded at different pump powers, we made a quantitative study of optical gain in all 7 CdSe/CdS samples. To provide an overview of the main trends, Figures 5a-c represent transient material gain spectra recorded for sample S1, S3 and S5, respectively. In all cases, a time delay of 3 ps was chosen as this delay generally yields the maximum gain. Considering the much longer time constants of multi-exciton decay (see Supporting Information S5), we can assume that at this point the initial carrier density is still present. In addition, the pump wavelength was set at 520 or 530 nm, *i.e.*, slightly below the CdS absorption edge, to ensure a constant excitation profile throughout the samples.

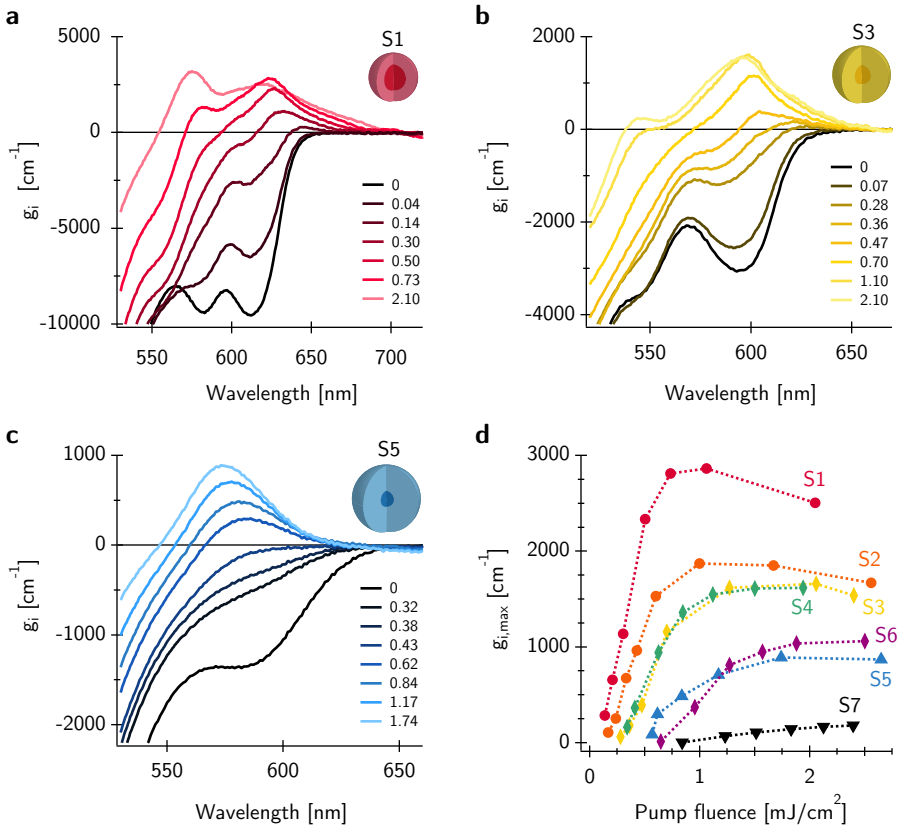

Figure 5: (a-c) Material gain spectra recorded at a delay of 3 ps for samples (a) S1, (b) S3, and (c) S5. The different traces have been recorded at different energy fluence as indicated. Fluence units are mJ/cm^{-2}. (d) Material gain maximum as a function of the pump energy fluence. Note that samples with the same core diameter have been represented by the same markers.

This implies that we created carriers in the highly degenerate shell and/or P states, from which they rapidly cool to occupy the band-edge states.

For all 3 spectra shown, we found that increasing the pump fluence brings the QD dispersions in a regime of net optical gain. At first, gain appears at around the $1S_h - 1S_e$ band-edge transition. Interestingly, in the case of the large core/thin shell sample S1, this initial gain band exhibits a redshift as compared to the band-edge transition, whereas for the small core/thick shell sample S5, the initial gain band is blue shifted. We will come back to this observation later. With increasing pump power, the gain band develops into a broad gain spectrum that can be up to 150 nm wide in the case of sample S1. Since this gain band

has the imprint of the higher energy $2S_h - 2S_e$ transition, we attribute this broadening of the gain spectrum to state filling of the higher-energy $2S_h$ hole level. Finally, the material gain spectra represented in Figures 5a-c indicate that for all samples studied, optical pumping hardly induces photoinduced absorption below the band gap, which has been observed before for Cd- and Pb-based QDs and assigned to light absorption by surface-trapped carriers or intraband transitions, respectively.[36,37] We thus conclude that the material gain as deduced from TA spectroscopy involves an intrinsic QD property, and not the net effect of stimulated emission and a counteracting photoinduced absorption.

In Figure 5d, we show the maximum of the material gain spectrum as a function of the pump fluence for all 7 samples studied. In line with Figure 2, we find that this maximum material gain first increases linearly and then levels off – or even slightly decreases – when the pump fluence is raised. The limiting material gain as obtained for all different in the corresponding gain cross section have been listed in Supporting Information S6. Comparing the saturation traces for S1 and S3 shown in Figure 5d with the gain spectra in Figures 5a and 5b, it follows that the gain saturates at pulse energies where gain through the higher energy $2S_h - 1S_e$ transition becomes possible. Hence, it seems that gain saturation is indeed due to the complete occupation of the band-edge states with electrons and holes.

Considering sets of samples with similar core sizes, *i.e.*, (S1; S2), (S3; S4; S6), and (S5; S7), Figure 5d confirms that increasing the shell volume for a given core size lowers the maximum gain. For example, whereas sample S1 exhibits a maximum material gain of $2800\,\mathrm{cm}^{-1}$, we only obtain a value of $1900\,\mathrm{cm}^{-1}$ for sample S2. Note that the influence of core and shell sizes can be dramatic. In the case of sample S7, which features the smallest core and the thickest shell, the material gain reaches not even $250\,\mathrm{cm}^{-1}$, *i.e.*, less than 10% of the material gain of sample S1. A first look at the threshold fluence – determined here at the pump wavelength – within these 3 sets of core/shell QDs suggests that an increase of the shell thickness comes with a higher threshold. Although a detailed comparison with the initial model predictions require an analysis at wavelengths shorter than the band-edge

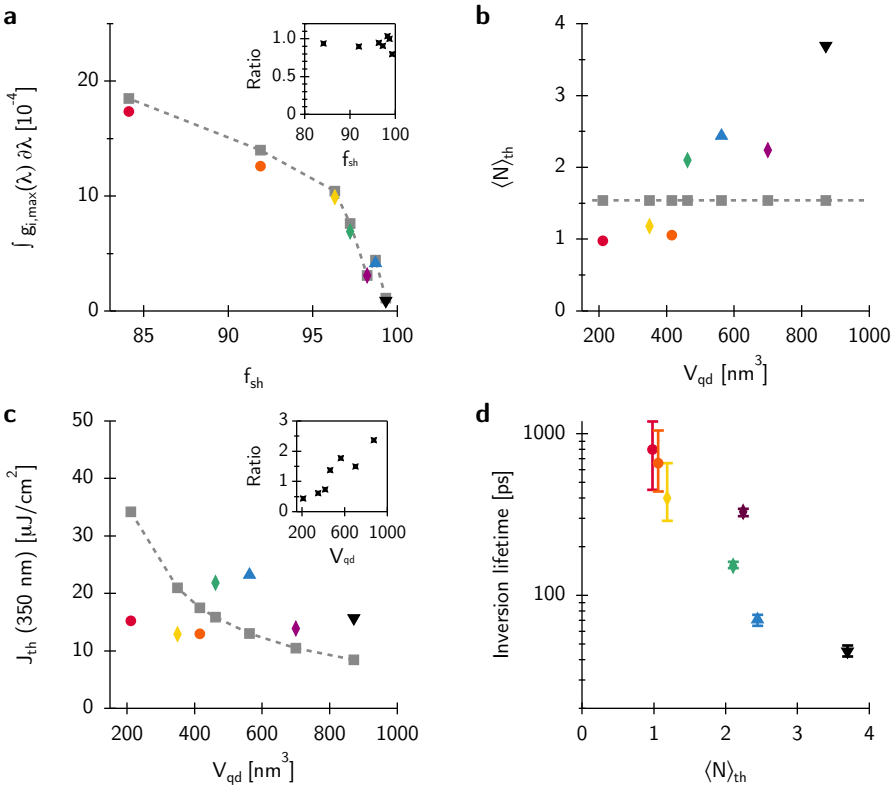

Figure 6: (a) Integrated maximum material gain *vs.* shell volume fraction as determined from (colored markers) experimental material gain maps and (grey markers) the intrinsic absorption coefficient spectrum. The inset shows the ratio of both numbers. (b-c) Estimated thresholds $J_{\mathrm{th}}(350\ \mathrm{nm})$ and $\langle N\rangle_{\mathrm{th}}$ as a function of V_{qd} as determined from (colored markers) experimental data and (gray markers) theoretical values. The latter are based on a fixed threshold occupation $\langle N\rangle_{\mathrm{th}}$=1.54 and the respective absorption cross sections (see Supporting Information S7). (d) The gain lifetime as a function of V_{qd}.

transition, this finding is unexpected since the cross section of the core transitions – and thus the threshold to reach a given occupation N – should be similar for similar cores.

Initial Model Validation

The initial model introduced to assess the impact of core/shell sizes on the gain characteristics anticipated first of all a reduction of the maximum material gain with increasing shell volume fraction (see Figure 2e). To single out optical gain associated with the band-gap transition and avoid possible artefacts due to spectral broadening or spectral shifts, we assessed this

prediction by integrating the material gain spectrum from the long wavelength side up to the gain maximum and doubling the resulting numbers. The results of this analysis are displayed in Figure 6a, were colored markers represent the experimental data based on gain spectra.

In agreement with the model, we find that the material gain systematically decreases with increasing shell volume fractions, up to the point where optical gain vanishes in the limit $f_{\mathrm{sh}} \to 1$. In addition, the grey squares in Figure 6a represent the similarly integrated intrinsic absorption coefficient for each sample, a number expected to yield the maximum material gain according to the initial model. As shown in the inset of Figure 6a, the ratio between the experimental and the theoretical maximum material gain is indeed close to one, falling in a narrow range around 1.0 for all samples bar S7. As can be seen in Figure 5d, the deviating ratio of 0.8 we found with S7 is most likely due to the pump power being insufficient to reach full saturation for this sample. Hence, in full agreement with the initial model, we conclude that the integrated intrinsic absorption coefficients provides an almost quantitative estimate of the maximum attainable material gain of a sample of CdSe/CdS QDs; a relation that makes that large-core/thin-shell QDs exhibit the largest material gain.

As a second point, the initial model predicted an inverse scaling of the gain threshold with the QD volume at pump wavelengths λ_{p} where both core and shell absorb light. The main assumption leading to this $1/V_{\mathrm{qd}}$ scaling of the gain threshold was that core/shell QDs have the same threshold occupation $\langle N \rangle_{\mathrm{th}}$, regardless of their morphology, which we estimated at $\langle N \rangle_{\mathrm{th}} = 1.54$. Figure 6b represents experimental threshold occupations as obtained from the data represented in Figure 5d (see Supporting Information S7 for details). Opposite from the initial assumption, indicated by the grey markers in Figure 5b, it follows that $\langle N \rangle_{\mathrm{th}}$ is markedly different for the various CdSe/CdS samples studied here. In the case of thin shell samples such as S1, S2 and S3, the experimental threshold occupation amounts to just 1.0 electron/hole pair per QD, *i.e.*, considerably smaller than expected, whereas it requires on average 3.7 electron-hole pairs to attain optical gain in the case of the thick

shell sample S7. These differences in threshold occupation make that the corresponding threshold fluences at wavelengths shorter than the CdS band-edge transition constitute a set of scattered numbers, ranging between 12 and 20 μJ/cm^2 (see Figure 6c). Hence, the expected pronounced threshold reduction for more voluminous QDs is absent for actual CdSe/CdS core/shell QDs.

To further assess the impact of the differences in threshold occupation on the optical gain characteristics of CdSe/CdS QDs, we looked at the time window during which optical gain persists after optical pumping. Characterizing this window by the time delay τ_g where the regime of optical gain disappears, we find that optical gain can last up to 800 ps in the case of the thin-shell sample S1, whereas optical gain has already disappeared after 45 ps in the case of the thick-shell sample S7, see Figure 6d. If indeed, as indicated by the gain threshold, optical gain in the latter sample requires higher-order multiexcitons, this dramatic collapse of the gain lifetime is to be expected. Multi-excitons recombine through Auger processes, which speed up significantly with increasing N. Hence, we conclude that thick shell CdSe/CdS core/shell QDs have multiple disadvantages as optical gain material. While they exhibit, as expected, a lower material gain, the higher threshold occupation makes that this drawback is not compensated by a lower threshold energy and brings the additional disadvantage of a shortened optical gain window.

Spectral Shifts in Photo-Excited CdSe/CdS Quantum Dots

As discussed above, we find that $\langle N \rangle_{\mathrm{th}}$ can be as low as 1 electron/hole pair for large core/thin shell QDs, whereas it raises to 3.7 for the thickest shell sample studied. To find out why the threshold occupation differs so much from the expected occupation of 1.54, we focus on the observation that the gain band initially develops at the red side of the band-edge transition for large-core/thin-shell QDs, such as S1, and at the blue side for small-core/thick-shell samples, such as S5. To understand this spectral variation of the gain band, we compare for each sample the linear absorbance spectrum A_0 with the absorbance spectrum A_1 of the

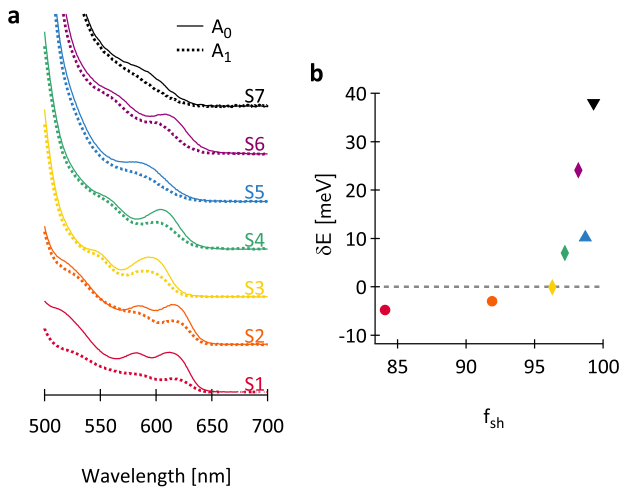

Figure 7: (a) Representation of (full lines) the absorbance spectra A_0 and (dotted lines) the absorbance spectra A_1 of all samples studied here. The absorbance spectra A_1 have been recorded by means of transient absorption spectroscopy at high pump fluences and long delays. (b) Shift δE between the energy of the $1S_h - 1S_e$-feature in the absorbance spectra A_0 and A_1.

same sample under conditions where each QD contains 1 electron-hole pair (see in Figure 7). We obtained the latter by adding to A_0 the change in absorbance recorded under conditions where at least 95% of the QDs contain a single electron-hole pair. In practice, this is achieved by using optical pulses that create an initial average exciton population of $\langle N \rangle \geq 3$ and a delay of 3 ns, to ensure that all multiexcitons have decayed.

Focusing first on the A_1-spectrum recorded on the large core/thin shell sample S1, one sees that the A_1-spectrum contains similar, yet slightly shifted features as compared to the A_0-spectra. A look at the different spectra directly shows that the exciton features in A_1 are redshifted as compared to A_0 in the case of sample S1, whereas they are blueshifted for thick shell samples such as S6 and S7. As discussed in the Supporting Information S8, these shifts can be quantified by either an explicit deconvolution of the spectra or by analyzing the second derivative of the absorbance spectrum. Figure 7b displays the resulting energy shifts as a function of f_{sh}, which confirms that samples S1 and S2 exhibit a redshifted biexciton transition ($\delta E < 0$), while this transition is increasingly shifted to the blue ($\delta E > 0$) in the case of the thicker shell samples S4 to S7. Such shifts have been attributed before

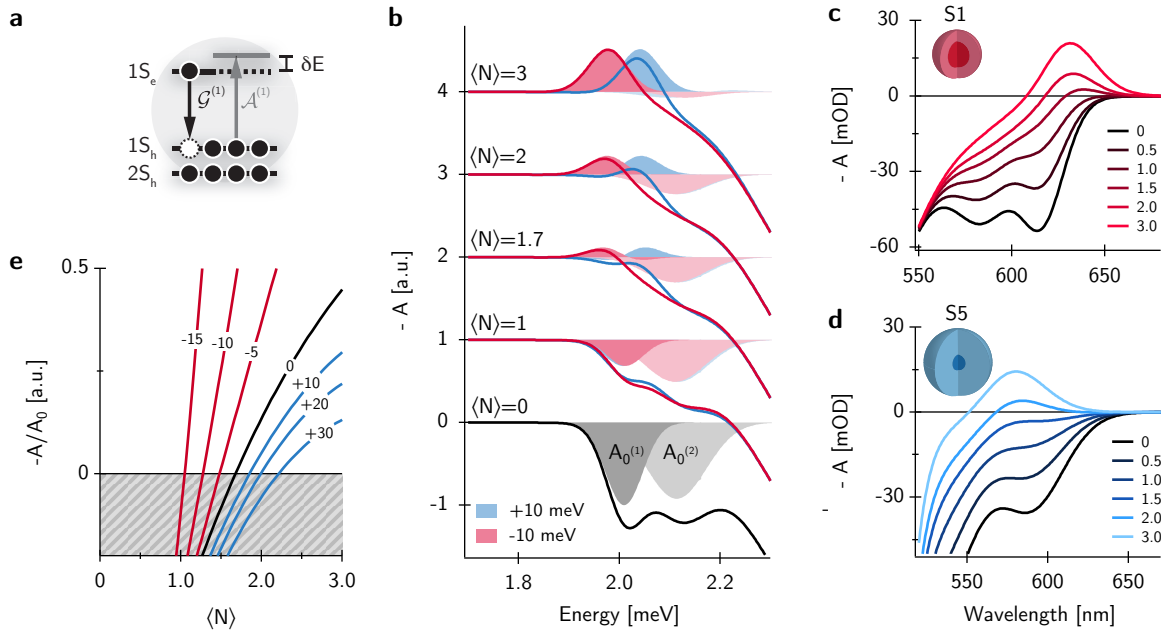

Figure 8: (a) Extended model, including an exciton-exction shift δE. (b) Nonlinear absorbance spectra in the case of (red line) attractive and (blue line) repulsive exciton-exciton interaction as a function of the average QD occupation $\langle N \rangle$. The filled areas represent the separate contributions $A^{(1)}$ and $A^{(2)}$, red for the case of attractive and in blue for repulsive exciton-exciton interactions, respectively. (c) Simulated nonlinear absorbance spectra as a function of the QD occupation $\langle N \rangle$. The simulations made use ot the A_0 spectrum of S1 and assumed an attractive exciton-exciton interaction of -15 meV. (d) The same as in (c), using the A_0 spectrum of S5 and assuming a repulsive exciton-exciton interaction of +15 meV. (e) Representation of normalized nonlinear absorbance $-A/A_0$ calculated at the wavelength were gain first appears as a function of $\langle N \rangle$ and for different exciton-exciton interactions as indicated.

to unbalanced Coulomb interactions between the different charge carriers forming a multi-exciton, which can shift the absorbance spectrum either to higher or lower energies depending on the characteristics of the nanostructure.[38–41] Already before, such shifts have been used to adjust optical gain thresholds,[42] and also here, we find that the spectral shift of the initial gain band is correlated to the biexciton Coulomb shift. For one thing, this finding confirms the idea that gain is due to biexciton or multiexciton transitions.

Extended Description of Optical Gain in Core/Shell Quantum Dots

Whereas experimental results on CdSe/CdS QDs and the initial model predictions agree in terms of gain coefficients, the marked differences between predicted and experimental gain threshold points to shortcomings in our initial description of optical gain. Considering Figures 5 and 7, two elements left out of the initial model are stimulated emission from higher energy transitions, different from the band-edge transition, and spectral shifts of the biexciton or multiexciton transitions. As we found, such shifts change from an attractive redshift for the samples featuring the lowest occupation threshold to a repulsive blueshift for the samples with the higher occupation threshold. Given these experimental insights, we extended the initial description of optical gain by including spectral shifts and higher energy transitions. Referring to Figure 8a, we modeled spectral shifts by means of a fixed shift δE that applies to the entire spectrum and that scales proportionally with the exciton occupation N.[41] In addition, we extended the simulated absorbance spectrum to a set of two transitions, *i.e.*, the band-edge labeled $A_0^{(1)}$ and a higher energy transition labeled $A_0^{(2)}$.

As outlined in Supporting Information S9, this extended model enabled us to simulate the non-linear absorbance spectrum of a QD dispersion using its linear absorbance spectrum as an input and taking the spectral shift δE as an adjustable parameter. To obtain an understanding of the way spectral shifts affect the absorbance of photo-excited QDs, and thus the possible development of a gain band, we took the measured A_0-spectrum of sample S1 as a starting point and imposed a positive and negative shift $|\delta E| = 10$ meV. As shown in Figure 8b, the spectral features $A_0^{(1)}$ and $A_0^{(2)}$ of the first and the second transition were obtained from a spectral deconvolution (see Supporting Information S8). Furthermore, a fixed background was included to account for higher energy transitions. The additional spectra in Figure 8b represent non-linear absorbance spectra simulated for different average occupations $\langle N \rangle$.

Focusing first on the case $\langle N \rangle = 1$, we use the filled areas to represent the net non-linear absorbances $A^{(1)}$ and $A^{(2)}$. Under these pump conditions, the non-linear spectra calculated

for either attractive or repulsive Coulomb interactions are highly similar, and no region of negative absorbance or gain is observed. Increasing the occupation to $\langle N \rangle = 1.7$, however, we see that the long wavelength side of the first exciton absorbance $A^{(1)}$ turns negative in the case of attractive exciton-exciton interactions. This results in an effective gain band, since the redshifted stimulated emission by bi-excitons does not overlap with other, absorbing transitions. In the case of repulsive Coulomb interactions, stimulated emission by biexcitons shows up at the short wavelength side of the first exciton absorbance. This blueshifted stimulated emission overlaps with the second exciton transition $A^{(2)}$ in residual, unexcited QDs. This counteracting absorbance makes that no net gain is achieved at these pump levels. Only by further increasing the occupation can this competition between stimulated emission and higher-energy absorbing transitions be overcome, as shown by the $\delta E = +10\,\mathrm{meV}$ spectrum simulated for $\langle N \rangle = 2$. Clearly, this finding agrees with the experimental correlation between spectral shifts and gain thresholds, where attractive exciton-exciton interactions concur with lower gain thresholds, whereas repulsive exciton-exciton interactions come with higher gain thresholds.

Figures 8c-d represents simulated spectra assuming Coulomb shifts $\delta E = -15\,\mathrm{meV}$ and $+15\mathrm{meV}$, where we used the absorbance spectrum of sample S1 and S5 as a reference, respectively. It can be clearly seen that including Coulomb shifts suffices to reproduce the main features of the experimentally determined gain characteristics, most notably the red shift or blue shift of the initial gain band, and the increased threshold to reach net stimulated emission in the case of repulsive Coulomb interactions. To further address the question of the gain threshold, Figure 8e displays the normalized non-linear absorbance at the wavelength where gain first appears as a function of the occupation $\langle N \rangle$. Here, calculations use the absorbance A_0 of sample S1 as a reference and the Coulomb shift is taken as an adjustable parameter. One clearly sees how an increasingly repulsive exciton-exciton interaction increases the threshold occupation, a trend caused by the increasing overlap between stimulated emission by the band-edge transition and counteracting absorbing transitions that are, initially, at a

higher photon energy. On the other hand, attractive exciton-exciton interactions can significantly lower the gain threshold, up to the point where $\langle N \rangle_{\mathrm{th}}$ drops below 1; a number often put forward as a hard limit for biexciton gain.[42]

Discussion

The combination of experimental findings and optical gain simulations based on the extended model indicates that two elements make large-core/thin-shell CdSe/CdS QDs the preferred core/shell combination in view of optical gain. First, by minimizing the dilution of the emitting CdSe core by the CdS shell, such QDs have the largest gain coefficients. In this respect, an interesting finding is that the integrated material gain matches the integrated intrinsic absorption coefficient for the band-edge transition, as expected for optical gain resulting from electron-hole pairs in the strong confinement regime. Second, large-core/thin-shell QDs exhibit attractive exciton-exciton interactions. Such interactions shift the stimulated emission by biexcitons away from competing absorbing transitions, which lowers the gain threshold. Importantly, both the maximization of the material gain by minimizing the shell volume and the positive impact of attractive exciton-exciton interactions on the gain threshold are model predictions independent of any specific characteristic of CdSe/CdS QDs. Hence, they can be taken as general design rules for optimizing QDs in view of optical gain.

In the literature, it has been argued that repulsive exciton-exciton interactions can be used to obtain net gain from stimulated emission by single excitons, hence leading to gain lifetimes comparable to the single exciton lifetime and possibly reducing the continuous wave lasing threshold.[42] As shown in Supporting Information S10, the model we developed here reproduces such a single exciton gain regime when we avoid any competing absorption. This requires that the band-edge transition is well-separated from the higher-energy transitions and that the exciton-exciton repulsion is sufficiently large compared to the transition linewidth. These conditions do not apply to the CdSe/CdS QDs studied here, yet they can

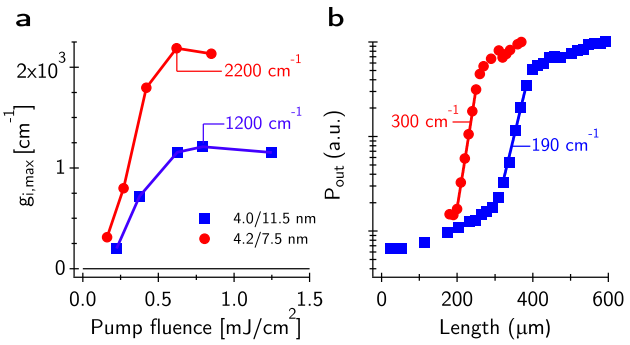

Figure 9: Comparsion of material gain and modal gain of two batches of CdSe/CdS QDs featuring (red circles) a 4.2 nm CdSe core and a 7.5 nm total diameter and (blue squares) a 4.0 nm CdSe core and a 11.5 nm total diameter. (a) Maximum material gain as a function of pump fluence. (b) Light output of SiN/QD/SiN strip waveguides of variable length pumped in the gain saturation regime. The modal gain as deduced from either curve is indicated.

be attained in core/shell QDs with a staggered, type II band alignment.[42] Even so, the approach to attain single exciton optical gain by repulsive exciton-exciton interactions has its limitations. As outlined in Supporting Information S10, a regime of single exciton gain by such a structure can only be reached when $P(1)/P(0)$ exceeds the product $g_e \times g_h$. Under femtosecond pumping, this requires an average occupation $\langle N \rangle$ significantly larger than 1. In addition, the material gain that stimulated emission by single excitons can provide is restricted to a fraction $1/(g_e g_h)$ of the intrinsic absorption coefficient of that transition at best. Hence, notwithstanding the special case of type II core/shell QDs, attractive exciton-exciton interactions are to be preferred to attain net optical gain in small footprint QD-based lasers.

Rather than the dilute QD dispersions studied here, QD lasers rely on densely packed QD films. In this respect, SiN/QD/SiN stacks provide a most useful testbed to quantify modal gain and lasing properties.[29] To highlight the relevance of the results obtained here for actual QD devices, we compared the modal gain of SiN/QD/SiN SiN/QD/SiN strip waveguides containing QDs with a 4.1 nm CdSe core and a total diameter of 7.5 nm with similar waveguides filled with QDs having a 4.0 nm core and an 11.5 nm total diameter as studied before by Zhu *et al.*[26] In line with the results shown in Figure 9a, the thinner shell QDs again exhibit the higher limiting material gain, attaining 2200 cm^{-1} in this case as

compared to 1200 cm^{-1} for the thicker shell QDs used by Zhu *et al.*[26] As outlined in Supporting Information S11, the SiN/QD/SiN strip waveguides exhibit a pronounced ASE feature under femtosecond pumping, which saturates with increasing pump power. Concomitantly, pumping waveguides of increasing length in the saturation regime leads to an exponential increase of the light output from the waveguide facet with increasing stripe length. As shown in Figure Figure 9b, we record the steeper increase – and thus the larger modal gain – for the waveguides containing the QDs with the thinner CdS shell. As outlined in the Supporting Information S11), the difference in modal gain, 300 cm^{-1} *versus* 190 cm^{-1}, can be traced back directly to the higher material gain of those QDs. This result not only validates the quantitative analysis of the material gain, but also confirms the conclusion that large core/thin shell QDs provide a higher modal gain and are thus the more optimal materials to realize small footprint QD-based lasers.

Conclusions

We have presented an experimental study on the relation between the gain characteristics of CdSe/CdS core/shell QDs and the core/shell morphology. In line with the prediction of a simple QD model, we find that the maximum material gain corresponds to the intrinsic absorption coefficient of the band-edge transition. This makes that large core/thin shell samples feature the higher material gain – reaching up to 2800 cm^{-1} for the best sample studied here. According to the same model, threshold fluences at pump photon energies above the CdS band gap should scale with the inverse of the QD volume. This prediction, however, is contradicted by the experimental results, which show little variation of the thresholds fluence as a function of core/shell sizes. This finding implies that thick shell QDs need more electron-hole pairs on average to reach transparency. At the same time, we find that such thick shell QDs show an increasingly repulsive exciton-exciton interaction. By means of simulated gain spectra, we show that the resulting blueshift of the multi-exciton

transitions accounts for this larger threshold occupation. As this comes with a pronounced shortening of the gain window, *i.e.*, the time span net optical gain can be maintained after photo-excitation, we conclude that CdSe/CdS QDs featuring a biexciton redshift, such as large-core/thin-shell CdSe/CdS structures, are preferred for optical gain applications. They combine a larger material gain with a lower threshold electron-hole pair occupation and a longer gain window. We believe such insights will be most valuable to guide future work to improve colloidal QDs for optical gain applications and develop optimized QD-lasers.

Methods

Synthesis of CdSe/CdS Core/Shell QDs. All samples used in this study consisted of oleate-capped CdSe/CdS core/shell QDs synthesized using a seeded-growth flash method as previously described in the literature.[31,32] First, wurtzite CdSe cores were synthesized from injections of trioctylphosphine selenide into cadmium phosphonate, with the size of the QDs being controlled by the reaction time. Next, CdS shells were grown by injecting a mixture of the CdSe cores and trioctlyphosphine sulfide into cadmium oleate. The thickness of the shell was controlled by changing the amounts of Cd and S in this second synthesis step. All samples were purified by mean of centrifugation using toluene and methanol as solvent and non-solvent respectively, then stored in toluene.

Transient Absorption Spectroscopy. Samples were excited using 110 femtosecond pump pulses at 520nm, created from the 800 nm fundamental (Spitfire Ace, Spectra Physics) through non-linear conversion in an OPA (Light Conversion TOPAS). Probe pulses were generated in a thin CaF_2 crystal using the 800 nm fundamental. The pulses were delayed relative to the pump using a delay stage with maximum delay of 6 ns. The probe spectrum in our experiments covers the UV-VIS window from 350 nm up to 750 nm. CdSe/CdS quantum dots were dispersed in an optically transparent solvent (toluene) and continuously stirred to avoid charging or photo-degradation. The pump wavelength and sample concentration

were chosen to obtain an optimal trade-off between having a good signal at the band-edge transitions, while still not having a too strong absorption at the pump-wavelength as to assure a uniform pumping of the sample.

The average number of absorbed photons (or equivalently created excitons) at time zero, noted as $\langle N \rangle$, can be calculated from the photon flux J_{ph}, the cuvette length L and the nanocrystal absorption cross section at the pump wavelength σ_{λ_p}: $\langle N \rangle = J_{ph} \times \sigma_{\lambda_p} \times \frac{1-e^{-\alpha_{0,\lambda_p} L}}{\alpha_{0,\lambda_p} L}$. The photon flux is calculated from the beam area, obtained through a Thorlabs CCD beam profiler, and defined as $A_{beam} = 2\pi \times \sigma_x \sigma_y$ where σ_i is the standard deviation in the $i = x, y$ direction.

Absorption and Photoluminescence Spectroscopy. Optical absorption and emission measurements were performed on diluted colloidal dispersions in toluene. Optical absorption spectra were measured with a Perkin Elmer L900 spectrophotometer. Steady-state and time-resolved PL spectra were excited by a pulsed laser diode (excitation wavelength 335 nm, pulse duration 250 ps, repetition rate 1 MHz). The PL spectra were collected with an Edinburgh standard spectrometer.

Supporting Information

The Supporting Information provides a definition of the material gain, and a description of the initial and extended model used to simulated optical gain. Moreover, additional sample characterization, including TEM-images, photoluminescence decay traces, and biexciton lifetimes are provided and details are given on the analysis of absorbance spectra, the calculation of fluence and occupation thresholds, and absorption cross sections. More details are included on the VSL experiments and finally, the optical gain model is used to evaluate the prospects of single exciton gain by repulsive exciton-exciton interactions.

Acknowledgement

ZH acknowledges support by the European Commission *via* the Marie-Sklodowska Curie action Phonsi (H2020-MSCA-ITN-642656) and the Marie Sklodowska-Curie Action Compass (H2020 MSCA-RISE-691185). ZH acknowledges the Research Foundation Flanders (project 17006602) and Ghent University (GOA no. 01G01513). PG acknowledges the FWO-Vlaanderen for a fellowship. TA acknowledges support by the European Commission *via* the Marie-Sklodowska Curie action NanoIntra (MSCA-IF-2015-702300).

References

1. Klimov, V. I.; Mikhailovsky, A. A.; Xu, S.; Malko, A.; Hollingsworth, J. A.; Leatherdale, C. A.; Eisler, H.-J.; Bawendi, M. G. Optical Gain and Stimulated Emission in Nanocrystal Quantum Dots. *Science* **2000**, *290*, 314–317.

2. Nurmikko, A. What Future for Quantum Dot-Based Light Emitters? *Nat. Nanotechnol.* **2015**, *10*, 1001–1004.

3. Kazes, M.; Lewis, D.; Ebenstein, Y.; Mokari, T.; Banin, U. Lasing from Semiconductor Quantum Rods in a Cylindrical Microcavity. *Adv. Mater.* **2002**, *14*, 317–321.

4. Malko, A. V.; Mikhailovsky, A. A.; Petruska, M. A.; Hollingsworth, J. A.; Htoon, H.; Bawendi, M. G.; Klimov, V. I. From Amplified Spontaneous Emission to Microring Lasing Using Nanocrystal Quantum Dot Solids. *Appl. Phys. Lett.* **2002**, *81*, 1303–1305.

5. Eisler, H.-J.; Sundar, V. C.; Bawendi, M. G.; Walsh, M.; Smith, H. I.; Klimov, V. Color-Selective Semiconductor Nanocrystal Laser. *Appl. Phys. Lett.* **2002**, *80*, 4614–4616.

6. Schaefer, J.; Mondia, J. P.; Sharma, R.; Lu, Z. H.; Susha, A. S.; Rogach, A. L.; Wang, L. J. Quantum Dot Microdrop Laser. *Nano Lett.* **2008**, *8*, 1709–1712.

7. Zavelani-Rossi, M.; Lupo, M. G.; Krahne, R.; Manna, L.; Lanzani, G. Lasing in Self-Assembled Microcavities of CdSe/CdS Core/Shell Colloidal Quantum Rods. *Nanoscale* **2010**, *2*, 931–935.

8. Dang, C.; Lee, J.; Breen, C.; Steckel, J. S.; Coe-Sullivan, S.; Nurmikko, A. Red, Green and Blue Lasing Enabled by Single-Exciton Gain in Colloidal Quantum Dot Films. *Nat. Nanotechnol.* **2012**, *7*, 335–339.

9. Grivas, C.; Li, C.; Andreakou, P.; Wang, P.; Ding, M.; Brambilla, G.; Manna, L.; Lagoudakis, P. Single-Mode Tunable Laser Emission in the Single-Exciton Regime from Colloidal Nanocrystals. *Nat. Comm.* **2013**, *4*, 2376.

10. Guzelturk, B.; Kelestemur, Y.; Akgul, M. Z.; Sharma, V. K.; Demir, H. V. Ultralow Threshold One-Photon- and Two-Photon-Pumped Optical Gain Media of Blue-Emitting Colloidal Quantum Dot Films. *J. Phys. Chem. Lett.* **2014**, *5*, 2214–2218.

11. She, C.; Fedin, I.; Dolzhnikov, D. S.; Demortiere, A.; Schaller, R. D.; Pelton, M.; Talapin, D. V. Low-Threshold Stimulated Emission Using Colloidal Quantum Wells. *Nano Lett.* **2014**, *14*, 2772–2777.

12. Grim, J. Q.; Christodoulou, S.; Di Stasio, F.; Krahne, R.; Cingolani, R.; Manna, L.; Moreels, I. Continuous-Wave Biexciton Lasing at Room Temperature Using Solution-Processed Quantum Wells. *Nat. Nanotechnol.* **2014**, *9*, 891–895.

13. Adachi, M. M.; Fan, F.; Sellan, D. P.; Hoogland, S.; Voznyy, O.; Houtepen, A. J.; Parrish, K. D.; Kanjanaboos, P.; Malen, J. A.; Sargent, E. H. Microsecond-Sustained Lasing from Colloidal Quantum Dot Solids. *Nat. Commun.* **2015**, *6*, 8694.

14. Fan, F.; Voznyy, O.; Sabatini, R. P.; Bicanic, K. T.; Adachi, M. M.; McBride, J. R.; Reid, K. R.; Park, Y.-S.; Li, X.; Jain, A.; Quintero-Bermudez, R.; Saravanapavanantham, M.; Liu, M.; Korkusinski, M.; Hawrylak, P.; Klimov, V. I.; Rosenthal, S. J.;

Hoogland, S.; Sargent, E. H. Continuous-Wave Lasing in Colloidal Quantum Dot Solids Enabled by Facet-Selective Epitaxy. *Nature* **2017**, *544*, 75–79.

15. Geiregat, P.; Houtepen, A. J.; Sagar, L. K.; Infante, I.; Zapata, F.; Grigel, V.; Allan, G.; Delerue, C.; Van Thourhout, D.; Hens, Z. Continuous-Wave Infrared Optical Gain and Amplified Spontaneous Emission at Ultralow Threshold by Colloidal HgTe Quantum Dots. *Nat. Mater.* **2018**, *17*, 35–42.

16. Klimov, V. I.; Mikhailovsky, A. A.; McBranch, D. W.; Leatherdale, C. A.; Bawendi, M. G. Quantization of Multiple Auger Rates in Semiconductor Quantum Dots. *Science* **2000**, *287*, 1011–1013.

17. Garcia-Santamaria, F.; Chen, Y.; Vela, J.; Schaller, R. D.; Hollingsworth, J. A.; Klimov, V. I. Suppressed Auger Recombination in "Giant" Nanocrystals Boosts Optical Gain Performance. *Nano Lett.* **2009**, *9*, 3482–3488.

18. Garcia-Santamaria, F.; Brovelli, S.; Viswanatha, R.; Hollingsworth, J. A.; Htoon, H.; Crooker, S. A.; Klimov, V. I. Breakdown of Volume Scaling in Auger Recombination in CdSe/CdS Heteronanocrystals: The Role of the CoreShell Interface. *Nano Lett.* **2011**, *11*, 687–693.

19. Bae, W. K.; Padilha, L. A.; Park, Y.-S.; McDaniel, H.; Robel, I.; Pietryga, J. M.; Klimov, V. I. Controlled Alloying of the Core/Shell Interface in CdSe/CdS Quantum Dots for Suppression of Auger Recombination. *ACS Nano* **2013**, *7*, 3411–3419.

20. Nasilowski, M.; Spinicelli, P.; Patriarche, G.; Dubertret, B. Gradient CdSe/CdS Quantum Dots with Room Temperature Biexciton Unity Quantum Yield. *Nano Lett.* **2015**, *15*, 3953–3958.

21. Pinchetti, V.; Meinardi, F.; Camellini, A.; Sirigu, G.; Christodoulou, S.; Bae, W. K.; De Donato, F.; Manna, L.; Zavelani-Rossi, M.; Moreels, I.; Klimov, V. I.; Brovelli, S.

Effect of Core/Shell Interface on Carrier Dynamics and Optical Gain Properties of Dual-Color Emitting CdSe/CdS Nanocrystals. *ACS Nano* **2016**, *10*, 6877–6887.

22. Park, Y. S.; Bae, W. K.; Baker, T.; Lim, J.; Klimov, V. I. Effect of Auger Recombination on Lasing in Heterostructured Quantum Dots with Engineered Core/Shell Interfaces. *Nano Lett.* **2015**, *15*, 7319–7328.

23. Todescato, F.; Fortunati, I.; Gardin, S.; Garbin, E.; Collini, E.; Bozio, R.; Jasieniak, J. J.; Della Giustina, G.; Brusatin, G.; Toffanin, S.; Signorini, R. Soft-Lithographed Up-Converted Distributed Feedback Visible Lasers Based on CdSe-CdZnS-ZnS Quantum Dots. *Adv. Func. Mater.* **2012**, *22*, 337–344.

24. Xie, W.; Stöferle, T.; Raino, G.; Aubert, T.; Bisschop, S.; Zhu, Y.; Mahrt, R. F.; Geiregat, P.; Brainis, E.; Hens, Z.; Van Thourhout, D. On-Chip Integrated Quantum-Dot/Silicon-Nitride Microdisk Lasers. *Adv. Mater.* **2017**, *29*, 1604866.

25. Lin, C. H.; Zeng, Q.; Lafalce, E.; Smith, M. J.; Malak, S. T.; Jung, J.; Yoon, Y. J.; Lin, Z.; Vardeny, Z. V.; Tsukruk, V. V. Large-Scale Robust Quantum Dot Microdisk Lasers with Controlled High Quality Cavity Modes. *Adv. Opt. Mater.* **2017**, *5*, 1700011.

26. Zhu, Y.; Xie, W.; Bisschop, S.; Aubert, T.; Brainis, E.; Geiregat, P.; Hens, Z.; Van Thourhout, D. On-Chip Single-Mode Distributed Feedback Colloidal Quantum Dot Laser under Nanosecond Pumping. *ACS Photonics* **2017**, *4*, 2446–2452.

27. le Feber, B.; Prins, F.; De Leo, E.; Rabouw, F. T.; Norris, D. J. Colloidal-Quantum-Dot Ring Lasers with Active Color Control. *Nano Lett.* **2018**, *18*, 1028–1034.

28. Hens, Z.; Moreels, I. Light Absorption by Colloidal Semiconductor Quantum Dots. *J. Mat. Chem.* **2012**, *22*, 10406–10415.

29. Xie, W.; Zhu, Y.; Bisschop, S.; Aubert, T.; Hens, Z.; van Thourhout, D.; Geiregat, P.

Colloidal Quantum Dots Enabling Coherent Light Sources for Integrated Silicon-Nitride Photonics. *IEEE J. Sel. Top. Quant.* **2017**, *23*, 8200913.

30. Efros, A.; Rosen, M.; Kuno, M.; Nirmal, M.; Norris, D.; Bawendi, M. Band-Edge Exciton in Quantum Dots of Semiconductors with a Degenerate Valence Band: Dark and Bright Exciton States. *Phys. Rev. B* **1996**, *54*, 4843–4856.

31. Cirillo, M.; Aubert, T.; Gomes, R.; Van Deun, R.; Emplit, P.; Biermann, A.; Lange, H.; Thomsen, C.; Brainis, E.; Hens, Z. Flash Synthesis of CdSe/CdS Core-Shell Quantum Dots. *Chem. Mater.* **2014**, *26*, 1154–1160.

32. Drijvers, E.; De Roo, J.; Geiregat, P.; Feher, K.; Hens, Z.; Aubert, T. Revisited Wurtzite CdSe Synthesis: A Gateway for the Versatile Flash Synthesis of Multishell Quantum Dots and Rods. *Chem. Mater.* **2016**, *28*, 7311–7323.

33. Cragg, G. E.; Efros, A. L. Suppression of Auger Processes in Confined Structures. *Nano Lett.* **2010**, *10*, 313–317.

34. Klimov, V. I. Spectral and Dynamical Properties of Multiexcitons in Semiconductor Nanocrystals. *Ann. Rev. Phys. Chem.* **2007**, *58*, 635–673.

35. Klimov, V. I.; McGuire, J. A.; Schaller, R. D.; Rupasov, V. I. Scaling of Multiexciton Lifetimes in Semiconductor Nanocrystals. *Phys. Rev. B* **2008**, *77*, 195324.

36. Malko, A.; Mikhailovsky, A.; Petruska, M.; Hollingsworth, J.; Klimov, V. Interplay Between Optical Gain and Photoinduced Absorption in CdSe Nanocrystals. *J. Phys. Chem. B* **2004**, *108*, 5250–5255.

37. De Geyter, B.; Houtepen, A. J.; Carrillo, S.; Geiregat, P.; Gao, Y.; ten Cate, S.; Schins, J. M.; Van Thourhout, D.; Delerue, C.; Siebbeles, L. D. A.; Hens, Z. Broadband and Picosecond Intraband Absorption in Lead-Based Colloidal Quantum Dots. *ACS Nano* **2012**, *6*, 6067–6074.

38. Nanda, J.; Ivanov, S. A.; Achermann, M.; Bezel, I.; Piryatinski, A.; Klimov, V. I. Light Amplification in the Single-Exciton Regime Using Exciton-Exciton Repulsion in Type-II Nanocrystal Quantum Dots. *J. Phys. Chem. C* **2007**, *111*, 15382–15390.

39. Rainò, G.; Stöferle, T.; Moreels, I.; Gomes, R.; Kamal, J. S.; Hens, Z.; Mahrt, R. F. Probing the Wave Function Delocalization in CdSe/CdS Dot-In-Rod Nanocrystals by Time-and Temperature-Resolved Spectroscopy. *ACS Nano* **2011**, *5*, 4031–4036.

40. Cihan, A. F.; Kelestemur, Y.; Guzelturk, B.; Yerli, O.; Kurum, U.; Yaglioglu, H. G.; Elmali, A.; Demir, H. V. Attractive *Versus* Repulsive Excitonic Interactions of Colloidal Quantum Dots Control Blue- to Red-Shifting (and Non-Shifting) Amplified Spontaneous Emission. *J. Phys. Chem. Lett.* **2013**, *4*, 4146–4152.

41. Geiregat, P.; Houtepen, A.; Justo, Y.; Grozema, F. C.; Van Thourhout, D.; Hens, Z. Coulomb Shifts upon Exciton Addition to Photoexcited PbS Colloidal Quantum Dots. *J. Phys. Chem. C* **2014**, *118*, 22284–22290.

42. Klimov, V. I.; Ivanov, S. A.; Nanda, J.; Achermann, M.; Bezel, I.; McGuire, J. A.; Piryatinski, A. Single-Exciton Optical Gain in Semiconductor Nanocrystals. *Nature* **2007**, *447*, 441–446.

Graphical TOC Entry